NUMERICAL ANALYSIS OF OSCILLATORY INSTABILITY OF BUOYANCY CONVECTION WITH THE GALERKIN SPECTRAL METHOD

A. Yu. Gelfgat and I. Tanasawa
Institute of Industrial Science, The University of Tokyo, Roppongi, Minato-ku, Tokyo, Japan

The Galerkin spectral method with basis functions previously introduced by Gelfgat [1] is applied for analysis of oscillatory instability of convective flows in laterally heated rectangular cavities. Convection of water and air in a square cavity, and convection of a low-Prandtl-number fluid in a square cavity, and a cavity with a ratio length / height of 4 are considered. Patterns of the most unstable perturbations of the stream function and the temperature are presented, and mechanisms of oscillatory instability are discussed. Comparison with other numerical investigations shows that the Galerkin method with divergent-free basis functions, which satisfy all the boundary conditions, needs fewer modes than other methods using discretization of the flow region.

INTRODUCTION

The problem of bifurcation from a stationary to an oscillatory state in convective flows was pointed out in the experimental work of Hurle et al. [2] and has been investigated by numerous authors for different fluids in different conditions. Numerical investigation of the threshold to oscillatory state is usually carried out with straightforward integration of nonstationary momentum and heat transfer equations, and localization of critical values of Grashof or Rayleigh numbers. Direct application of stability analysis is possible only in the simplest cases, when initial stationary flow may be obtained analytically [3] or perturbations of a convective flow are of a supposed known spatial structure, for example, spatial-periodic [4]. In general, when initial stationary flow must be obtained numerically, and a set of all possible perturbations have to be considered, application of the stability theory will lead to an eigenvalue problem of very high order. Namely, the order of the eigenvalue problem is equal to the number of unknown scalar variables used by a numerical method for approximation of the solution: number of unknown functions multiplied by number of discretization elements (nodes of grid, finite elements, or collocation points). Linear stability analysis was applied together with the finite element method for investigation of oscillatory instability of convec-

Received 26 April 1993; accepted 2 July 1993.
The authors wish to acknowledge the Ministry of Education, Science and Culture of Japan, and Japan Society for Promotion of Science for providing support for this research (grant 92024).
Address correspondence to I. Tanasawa, Institute of Industrial Science, The University of Tokyo, 7-22-1 Roppongi, Minato-ku, Tokyo, Japan.

Numerical Heat Transfer, Part A, 25:627–648, 1994

1040–7782/94 $10.00 + .00

NOMENCLATURE

A	aspect ratio ($= L/H$)	t	time, s
$A_{mk}, B_{mkl}, F_m, S_{mk}$	matrices defining the dynamical system	T_i, U_i	Chebyshev polynomials
		v	velocity, m s^{-1}
$A^*_{mk}, B^*_{mkl}, F^*_m$	matrices multiplied by $(S_{mk})^{-1}$	x, y	Cartesian coordinates, m
		X^0	stationary solution of the dynamical system
$c_{ij}(t), d_{ij}(t), X_i(t)$	time-dependent Galerkin coefficients	X_E	eigenvector of the dynamical system
f	frequency of oscillations, s^{-1}	β	volume expansion coefficient, K^{-1}
g	gravitational acceleration, m s^{-2}	θ	temperature, K
Gr	Grashof number ($= g\beta\Delta\theta H^3/\nu^2$)	λ	eigenvalue of the dynamical system
H	height of the cavity, m	ν	kinematic viscosity, $m^2\ s^{-1}$
J_{mk}	Jacobi matrix		
L	length of the cavity, m	$\varphi_{ij}(x, y)$	Galerkin-based velocity
Nu_0	Nusselt number at $x = 0$	χ	thermal diffusivity, $m^2\ s^{-1}$
p	pressure, Pa	ψ	stream function, $m^2\ s^{-1}$
Pr	Prandtl number ($= \nu/\chi$)		
$q_{ij}(x, y)$	Galerkin-based temperature	**Subscripts**	
Ra	Rayleigh number ($=$ Gr Pr)	cr	critical value
		max	maximum value

tion in rectangular cavities by Winters [5–7]. Winters showed that when stability analysis can be applied, it provides more effective calculation of critical parameters than any other methods using straightforward time integration.

However, the possibilities of applying the stability analysis for investigation of convective flows remain strongly restricted because of the very large order of the eigenvalue problems to be solved. It is clear that the number of unknown scalar variables cannot be sufficiently decreased if any discretization of the flow region is necessary. On the other hand, methods of weighted residuals with trial functions defined in the whole flow region allow use of fewer unknown scalars if the system of trial functions is properly chosen [4, 8, 9].

This paper investigates instability of stationary convective flows in confined regions using the Galerkin spectral method together with linear stability analysis. The system of basis functions for a Galerkin series of velocity and temperature was introduced by Gelfgat [1]. It was shown [1] that the Galerkin spectral method with basis functions satisfying all the boundary conditions and the continuity equation allows us to obtain accurate results with rather short truncated series. Thus, comparison with known theoretical and numerical data showed that the Galerkin series with six to nine basis functions in each spatial direction allow us to obtain accurate approximations for stationary buoyancy and thermocapillary convection in rectangular cavities for moderate values of Grashof and Marangoni numbers. All the results obtained in Ref. [1] relate to flows with simple spatial structure, without

thin boundary layers, and small-scale vortices in the core flow. It is obvious that calculation of convective flows with more complicated structures requires longer Galerkin series. In this paper we present results of calculations with 20–30 basis functions in each spatial direction for two problems of oscillatory instability of convective flows: (1) oscillatory instability of convection of low-Prandtl-number fluid in laterally heated rectangular cavities with length/height of 4 and (2) oscillatory instability of convection of low-Prandtl-number fluid, air, and water in a laterally heated square cavity. In spite of particular theoretical interest, these two problems are accepted as common tests for comparison of different numerical methods.

Application of the linear stability theory allows us to obtain patterns of the most unstable perturbation, which is described by the eigenvector corresponding to the dominating eigenvalue of the linearized equations. The spatial patterns of the most unstable perturbations are used to discuss physical mechanisms of the instability onset.

FORMULATION OF THE PROBLEM

Convection of the incompressible Boussinesq fluid in a rectangular cavity $0 \le x \le A, 0 \le y \le 1$ is considered. The convective flow is described by the momentum, energy, and continuity equations:

$$\frac{\partial \mathbf{v}}{\partial t} + (\mathbf{v}\nabla)\mathbf{v} = -\nabla p + \Delta \mathbf{v} + \mathrm{Gr}\,\theta e_y \tag{1}$$

$$\frac{\partial \theta}{\partial t} + (\mathbf{v}\nabla)\theta = \frac{1}{\mathrm{Pr}}\Delta\theta \tag{2}$$

$$\nabla \mathbf{v} = 0 \tag{3}$$

Here $\mathbf{v}$ is fluid velocity, θ is temperature, p is pressure, $\mathrm{Gr} = g\beta\Delta H^3/\nu^2$ is the Grashof number, $\mathrm{Pr} = \nu/\chi$ is the Prandtl number, $A = L/H$ is the aspect ratio, g is the acceleration gravity, β is the thermal expansion coefficient, $\Delta\theta$ is the characteristic temperature difference, ν is the kinematic viscosity, χ is the thermal diffusivity, and L and H are the characteristic length and height of the cavity, respectively.

Vertical boundaries of the cavity are rigid and isothermal:

$$\mathbf{v}(x = 0) = \mathbf{v}(x = A) = 0 \qquad \theta(x = 0) = 1 \qquad \theta(x = A) = 0 \tag{4}$$

Horizontal boundaries are considered to be adiabatic or perfectly conducting, the lower boundary is rigid, and the upper boundary is rigid or stress free:

$$\theta(y = 0,1) = 1 - x \qquad \frac{\partial\theta}{\partial y}(y = 0,1) = 0 \tag{5}$$

$$\begin{aligned} \mathbf{v}(y = 0) &= 0 & \mathbf{v}(y = 1) &= 0 \\ \frac{\partial v_x}{\partial y}(y = 1) &= 0 & v_y(y = 1) &= 0 \end{aligned} \tag{6}$$

NUMERICAL PROCEDURE

Solution of Eqs. (1)–(6) is approximated as a truncated series:

$$\mathbf{v} = \sum_{i=1}^{N}\sum_{j=1}^{M} c_{ij}(t)\boldsymbol{\varphi}_{ij}(x,y) \qquad \theta = (1-x) + \sum_{i=1}^{K}\sum_{j=1}^{L} d_{ij}(t)q_{ij}(x,y) \tag{7}$$

Functions φ_{ij} and q_{ij} are defined as linear superpositions of the Chebyshev polynomials of the first and second type T_n and U_n:

$$T_n(x) = \cos[n\arccos(2x-1)] \qquad U_n(x) = \frac{\sin[(n+1)\arccos(2x-1)]}{\sin[\arccos(2x-1)]} \tag{8}$$

in the following form:

$$q_{ij}(x,y) = \sum_{l=0}^{2} \alpha_{il} T_{i+l}\left(\frac{x}{A}\right) \sum_{l=0}^{2} \beta_{jl} T_{j+l}(y) \tag{9}$$

$$\boldsymbol{\varphi}_{ij}(x,y) = \left\{ \begin{array}{l} \displaystyle\sum_{l=0}^{4} \frac{f_{il}}{2(i+l)} T_{i+l}\left(\frac{x}{A}\right) \sum_{l=0}^{4} g_{jl} U_{j+l-1}(y) \\ \displaystyle -\sum_{l=0}^{4} f_{il} U_{i+l-1}\left(\frac{x}{A}\right) \sum_{l=0}^{4} \frac{g_{jl}}{2(j+l)} T_{j+l}(y) \end{array} \right\} \tag{10}$$

Polynomials T_n and U_n are related by formula $(d/dx)T_{i+1}(x) = 2(i+1)U_i(x)$, which provides zero divergence of functions φ_{ij} and analytical fulfillment of the continuity equation, Eq. (3).

Coefficients α_{il}, β_{il}, f_{il}, and g_{il} are defined by substitution of the expressions Eqs. (9) and (10) in boundary conditions Eqs. (4)–(6). For each i and j this gives two linear homogeneous equations for every three coefficients α_{il} or β_{jl} ($l = 0, 1, 2$), and four linear homogeneous equations for every five coefficients f_{il} or g_{il} ($l = 0, 1, 2, 3, 4$). After addition, using fixed values for coefficients corresponding to $l = 0$ ($\alpha_{il} = \beta_{il} = f_{il} = g_{il} = 1$), one can obtain completely definite systems of linear algebraic equations for each group of coefficients. After solution of these systems, a dependence of all the coefficients on numbers i, j, l will be obtained. Formulas for the coefficients α_{il}, β_{il}, f_{il}, and g_{il} are given in the appendix.

Functions φ_{ij} and q_{ij} are bases in the functional spaces containing divergent-free functions satisfying all the homogeneous boundary conditions of the problem. In other words, the approximate solution Eq. (7) is localized in the subspace of divergent-free functions satisfying all the boundary conditions before the computational process starts. It will be shown that this may improve the convergence and decrease the number of modes necessary for approximation of the solution.

Using Eqs. (9) and (10), one can construct different systems of trial and test functions for the method of weighted residuals (for details, see Ref. [10]). Several numerical experiments using different systems of the test and trial functions showed that convergence is better in the case when test and trial systems coincide,

i.e., in the case of the Galerkin method. In all calculations described below, we used only the Galerkin formulation. The same bases were used for the expansions Eq. (7) and for projections of residuals. Both test and trial functions here are called "basis functions."

To complete formulation of the Galerkin method, we define inner products as

$$\langle f_1, f_2 \rangle = \int_V f_1 f_2 \, dV \qquad \langle \mathbf{u}_1, \mathbf{u}_2 \rangle = \langle u_1^{(x)}, u_2^{(x)} \rangle + \langle u_1^{(y)}, u_2^{(y)} \rangle \tag{11}$$

After substitution of series Eq. (7) in Eqs. (1) and (2) and calculation of all the necessary inner products, the considered problem is reduced to a system of ordinary differential equations for definition of the time-dependent coefficients $c_{ij}(t)$ and $d_{ij}(t)$. The system may be written in the following form (here and after summation over repeating indices is supposed):

$$S_{mk} \frac{dX_k(t)}{dt} = A_{mk} X_k(t) + B_{mkl} X_k(t) X_l(t) + F_m \tag{12}$$

where $m = \overline{1, KL + MN}$ and X_k is one of the coefficients $c_{ij}(t)$ or $d_{ij}(t)$:

$$\begin{aligned} X_{L(i-1)+j} &= d_{ij} \qquad i = 1, K \qquad j = 1, L \\ X_{LK+M(i-1)+j} &= c_{ij} \qquad i = \overline{1, N} \qquad j = \overline{1, M} \end{aligned} \tag{13}$$

The Chebyshev weight $\rho(x) = (x - x^2)^{-1/2}$ is not used in the definition of the inner products, Eq. (11), because unit weight $\rho(x) = 1$ provides two important properties of the resulting equation, Eq. (12). First, any divergent-free function φ with vanishing normal to the boundary component is orthogonal to the gradient of any scalar function p:

$$\int_V \varphi \cdot \nabla p \, dV = 0 \tag{14}$$

This means that pressure is eliminated from the Navier-Stokes equation, Eq. (1), by the Galerkin procedure only, and the resulting equation, Eq. (12), does not contain any equation without time derivative. Second, conservative properties

$$\int_V (\mathbf{v}\nabla)\mathbf{v} \cdot \mathbf{v} \, dV = \int_V (\mathbf{v}\nabla)\theta \cdot \theta \, dV = 0 \tag{15}$$

are introduced in Eq. (12) as equality $B_{mkl} X_m X_k X_l = 0$ for any current values of variables X_k. This means that all the dissipative properties of Eq. (12) are determined by matrix A_{mk}, which contains projections of the dissipative terms of Eqs. (1) and (2) on the phase space with coordinates X_k.

Matrix S_{mk} in Eq. (12) is not diagonal because of the nonorthogonality of the basis functions. It depends on the boundary conditions and the aspect ratio but not

on the Grashof and Prandtl numbers. So for a problem with fixed aspect ratio, matrix S_{mk} may be inversed and the right-hand side of Eq. (12) may be multiplied by the inverse matrix only once for all values of Pr and Gr. As a result, Eq. (12) is replaced by a modified system with resolved time derivatives:

$$\frac{dX_m(t)}{dt} = A^*_{mk} X_k(t) + B^*_{mkl} X_k(t) X_l(t) + F^*_m \tag{16}$$

where the asterisk (*) corresponds to a matrix from Eq. (12) multiplied by S^{-1}_{mk}.

A completely explicit form of Eq. (16) allows us to use standard numerical methods developed for systems of ordinary differential equations both for obtaining its stationary and nonstationary solutions and investigation of the stability of solutions. Namely, the stationary solution X^0 of the system Eq. (16) is unstable if the Jacobi matrix,

$$J_{mk} = \frac{\partial X_m}{\partial X_k} = A^*_{mk} + (B^*_{mkl} + B^*_{mlk}) X_l \tag{17}$$

at $X = X^0$ has at least one eigenvalue λ with $\mathrm{Re}\,\lambda > 0$. Thus the investigation of stability for given Pr and A requires the determination of such values of Gr that provide zero real part $\mathrm{Re}\,\lambda = 0$ of the dominating eigenvalue λ (eigenvalue with the maximal real part). The imaginary part $\mathrm{Im}\,\lambda$ of the dominating eigenvalue gives an estimation of cycle frequency of the oscillatory flow that develops after the onset of instability.

Eigenvector X_E, corresponding to the dominating eigenvalue λ, such as $\mathrm{Re}\,\lambda = 0$, defines the most unstable perturbation of the system Eq. (16). The most unstable perturbation of the convective flow may be calculated using series Eq. (7) with coefficients c_{ij} and d_{ij} defined as components of the eigenvector X_E from Eq. (13).

Equations (16) and (17) are completely explicit with respect to the time derivatives and the components of the Jacobi matrix, and their right-hand parts contain only matrix operations. Effective vectorization of the computational process may be easily reached if there is enough computer memory to keep all the components of matrixes A, B, and F. Due to nonorthogonality of the basis functions, these matrices are completely filled by nonzero elements. For example, matrix B_{mkl} corresponding to the nonlinear terms of the Boussinesq equations, contains $N^3/2$ nonzero elements, where N is the total number of modes. Thus the total number of modes that may be used in the computations is strongly restricted. This may be considered the most serious disadvantage of the numerical method discussed.

In the computations described, stationary solutions of the system Eq. (17) were calculated with the Newton method, and eigenvalues of the Jacobi matrix were computed using QR decomposition. It was possible to use no more than 900 modes in total. One run of the Fortran code contained calculation of stationary solutions, analysis of their stability, localization of the critical Grashof number

(Gr_{cr}), and calculation of the eigenvector, which needed less than 3 min on the Hitachi supercomputer S3800/480.

Stream function ψ and Nusselt number Nu_0 computed at the boundary $x = 0$ are used below for the description of the results. Both were calculated from the analytical formulas following from Eqs. (7)–(10).

$$\psi = \sum_{l=0}^{4} \frac{f_{il}}{2(i+l)} T_{i+l}\left(\frac{x}{A}\right) \sum_{l=0}^{4} \frac{g_{jl}}{2(j+l)} T_{j+l}(y) \qquad v_x = \frac{\partial \psi}{\partial y} \qquad v_y = -\frac{\partial \psi}{\partial x} \tag{18}$$

$$Nu_0 = \int_0^1 \left(\frac{\partial \theta}{\partial x}\right)_{x=0} dy = 2 \sum_{l=0}^{2} (-1)^{i+l} (i+l)^2 \alpha_{il} \sum_{l=0}^{2} \beta_{jl} \langle T_{j+l}, T_0 \rangle \tag{19}$$

RESULTS

Convection of Low-Pr Fluid in a Long Horizontal Cavity (GAMM test)

The problem considered is that of oscillatory instability of convection of fluid with Pr = 0.015 in a laterally heated rectangular cavity with aspect ratio $A = L/H = 4$. This problem was accepted as the GAMM test for comparison of different numerical methods [11]. According to Ref. [11], four types of boundary conditions on the horizontal boundaries are considered: the R_c-R_c case for rigid, perfectly conducting horizontal boundaries; the R_a-R_a case for rigid adiabatic horizontal boundaries; the R_c-F_c case for perfectly conducting horizontal boundaries, where the lower boundary is rigid and the upper boundary is stress free; and the R_a-F_a case for adiabatic horizontal boundaries, where the lower boundary is rigid and the upper boundary is stress free. In this section, a modified definition of the Grashof number, $Gr^* = Gr\ H/L$, is used to make comparisons with other works more apparent.

In cases R_a-R_a and R_c-R_c the convective flow is symmetric with respect to rotation 180° around the center of the cavity. This symmetry appears in the basis functions as a result of symmetric homogeneous boundary conditions in such a way that one half of the functions is symmetric and the other half is antisymmetric:

$$\varphi_{ij}(x,y) = (-1)^{i+j} \varphi_{ij}(1-x, 1-y) \qquad q_{ij}(x,y) = (-1)^{i+j+l} q_{ij}(1-x, 1-y) \tag{20}$$

This property allows us to exclude half the modes when the stationary solution is calculated. Antisymmetric modes cannot be excluded from the analysis of stability because instability may be connected with a break of symmetry. In both cases R_a-R_a and R_c-R_c, instability analysis showed that the most unstable perturbation is also symmetric. This is in complete agreement with several straightforward calculations [12–14, 8], which show preservation of symmetry in instantaneous patterns of supercritical flows, as well as with patterns of eigenvectors obtained with bifurcation analysis by Winters [6, 7].

Table 1. Results Obtained for the R_c-R_c Case and Comparison with Results of Previous Work: GAMM Test, Cavity with $L/H = 4$, $Gr^* = Gr\ H/L$, and $Pr = 0.015$

	Present work			Previous work			
	26 × 10	28 × 12	30 × 14	81 × 321 Uniform finite difference mesh [15]	From 30 × 16 to 40 × 30 Chebyshev modes [8, 9]	35 × 101 Non uniform finite difference mesh [12]	60 × 24 Finite elements and bifurcation analysis [6, 7]
				$Gr^* = 25{,}000$, stationary solution			
Ψ_{max}	0.4338	0.4335	0.4337	0.4334	0.4337	0.4169	—
U_{max} $(x = 1)$	0.7042	0.7052	0.7055	0.7037	0.706	—	—
V_{max} $(y = 0.5)$	0.5703	0.5716	0.5717	0.5684	0.568	—	—
				Oscillatory instability onset			
$Gr^*_{cr} \times 10^{-4}$	2.775	2.826	2.83	—	2.8–2.85	2.5–2.85	2.8153
f_{cr}	17.249	17.517	17.529	—	17.45	< 17.63	17.445

Examples of convergence of the considered Galerkin method for case R_c-R_c and comparison with the results of other authors are shown in Table 1. As is seen from the table, 26 basis functions in the x direction and 10 functions in the y direction provide two correct digits both for the stationary solution with $Gr^* = 25{,}000$ and for values of the Gr_{cr} and the critical frequency (f_{cr}). Increasing the number of modes up to 30 × 14 functions approves convergence of the method. All the results are in good agreement with the results of previous work.

It should be noted (see Table 1) that the total number of scalar unknowns necessary in the present computations was noticeably less than the total number of unknowns in other numerical analyses using finite difference or finite element methods. Pulicani et al. [8, 9] used the tau spectral method with Chebyshev polynomials as basis functions, and obtained accurate results for subcritical stationary flow with 30 × 16 modes. But for accurate computation of the critical Grashof number, 40 × 30 Chebyshev polynomials were necessary. Winters [7] also reported that accurate prediction of Gr_{cr} requires a finer grid than calculation of the stationary flow only.

Analysis of the numerical solutions obtained in this work with a different number of Galerkin modes showed that the main difficulty both in case R_a-R_a and case R_c-R_c is related to accurate determination of the position of two smaller convective vortices (see Figure 1). This may be a sequence of minimization of error used in the Galerkin method: spatially distributed error is minimized on average, so local errors may remain relatively large even if the averaged error is small.

Results of stability analysis and comparison with previous works are shown in Table 2. In cases R_a-F_a and R_c-F_c there are no symmetrical properties and all the Galerkin coefficients have nonzero values. This produces stronger restrictions for truncation of the Galerkin series. On the other hand, the spatial structure of the convective flow in these two cases is simpler than in the case of two rigid horizontal boundaries (see Figure 2), which allows us to obtain comparable results with 24 × 10 Galerkin modes.

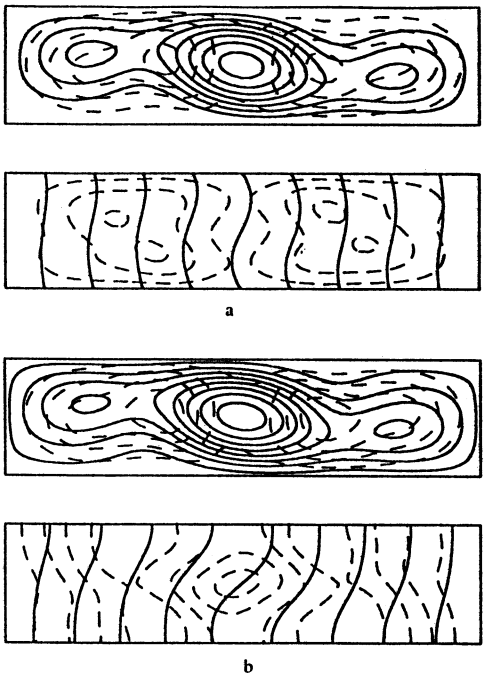

Figure 1. Streamlines and isotherms (solid lines), and the most unstable perturbations of the stream function and the temperature (dashed lines) for (a) case R_c-R_c, Gr = 2.835×10^4, and (b) case R_a-R_a, Gr = 3.330×10^4, at Pr = 0.015, 30×14 Galerkin modes.

Table 2. Comparison of Critical Grashof Numbers and Frequencies of Oscillations with Results of Previous Work: GAMM Test, Cavity with $L/H = 4$, $Gr^* = Gr\ H/L$, Pr = 0.015

	Present work		Previous work			
	24×10	30×14	60×24 Finite element and bifurcation analysis [6, 7]	35×101 and 41×121 Non-uniform finite difference mesh [12]	From 40×16 to 50×20 Pseudo-spectral Chebyshev modes [13]	From 30×16 to 40×30 Chebyshev modes [8, 9]
R_c-R_c case $Gr^*_{cr} \times 10^{-4}$	—	2.83	2.8153	2.5×2.85	2.7875	2.8×2.85
f_{cr}	—	17.529	17.445	< 17.63	17.27	17.45
R_a-R_a case $Gr^*_{cr} \times 10^{-4}$	—	3.330	3.3002	3.25–3.35	—	3.30–3.35
f_{cr}	—	19.765	19.656	19.06–20	—	< 19.72
R_c-F_c case $Gr^*_{cr} \times 10^{-4}$	1.477	—	1.4767	1.475–1.5	1.365	1.40–1.47
f_{cr}	12.814	—	12.818	< 12.94	12.33	< 13.07
R_a-F_a case $Gr^*_{cr} \times 10^{-4}$	1.937	—	1.6598	1.90–1.95	—	1.85–1.90
f_{cr}	14.962	—	13.557	< 15.01	—	< 14.91

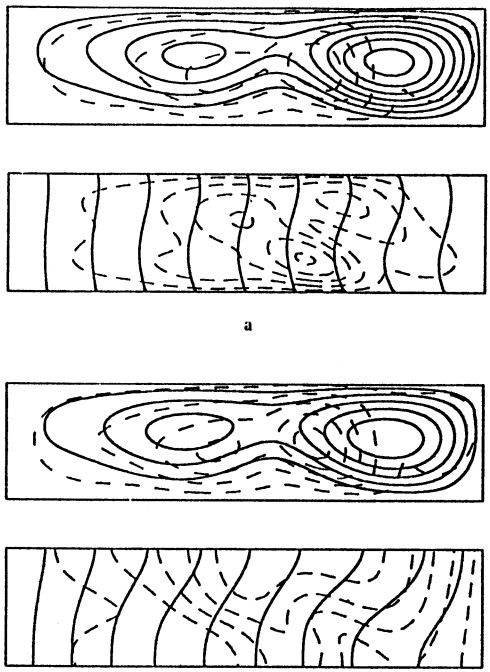

Figure 2. Streamlines and isotherms (solid lines), and the most unstable perturbations of the stream function and the temperature (dashed lines) for (a) case R_c-F_c, Gr = 1.477×10^4, and (b) case R_a-F_a, Gr = 1.937×10^4, at Pr = 0.015, 24×10 Galerkin modes.

Streamlines, isotherms, and patterns of the most unstable perturbations for Gr_{cr} in cases R_a-R_a and R_c-R_c are shown in Figure 1. Solid lines are used for plotting the streamlines and isotherms, and dashed lines for the isolines of the most unstable perturbations. In the case of oscillatory instability, the eigenvector of the linearized system has complex components. Since the eigenvector is defined within multiplication by a complex constant, only the absolute value of the eigenvector has physical meaning and is plotted.

As is seen from Figure 1, patterns of the streamlines as well as patterns of the stream function perturbations are similar in both cases R_a-R_a and R_c-R_c. This leads to the conclusion that in both cases, convective instability is connected with instability of fluid flow, in spite of different patterns of the perturbation of the temperature. Maximal values of the stream function perturbations are located at the periphery of the central vortex. It may be supposed that instability is caused by interaction between the central vortex and smaller vortices. Such a supposition corresponds to results of analysis of slightly supercritical flows made by Winters [5, 6], and straightforward solutions by Pulicani et al. [8, 9] and Ben Hadid and Roux [12] who reported that synchronous oscillations of smaller vortices existed together with pulsations of the central vortex. The same oscillations were obtained in the case Pr = 0, which shows a completely hydrodynamical origin of the instability. This conclusion was confirmed in this work by analysis of patterns of the stream function perturbation for Pr = 0, which was found to be the same as for Pr = 0.015.

Thus, instability mechanisms for different thermal boundary conditions are the same in both cases R_a-R_a and R_c-R_c. On the other hand, thermal boundary

conditions influence fluid velocity, and thus the Gr_{cr}. Oscillations of the temperature in these cases are sequences of the velocity oscillations. But, as one can conclude from the patterns of temperature perturbations, spatial distributions of the amplitude oscillations of the temperature are different for different boundary conditions. In case R_a-R_a (see Figure 1b) the most intensive oscillations of the temperature may be expected in the center of the cavity, where the maximum perturbation is located. But in case R_c-R_c, maxima of the temperature perturbation are shifted from the center toward the boundaries, and at least two maxima in spatial distribution of the oscillation amplitude may be expected.

Patterns of convective flows corresponding to Gr_{cr} and the most unstable perturbations for the R_a-F_a and R_c-F_c cases are shown in Figure 2. One can see from the figure that for a stress-free upper boundary the same conclusion about instability of the fluid flow takes place: patterns of the streamlines as well as patterns of their perturbations are similar in both cases. The same patterns were obtained in the case of Pr = 0. As in the case of rigid upper boundary maxima of stream functions, perturbations are located at the periphery of two vortices. Oscillations of these vortices were reported by Behnia and de Vahl Davis [15] in the case of Pr = 0, and by Pulicani et al. [9] for cases Pr = 0 and R_a-F_a, Pr = 0.015. These results are in agreement with the pattern of the most unstable perturbation obtained in this work.

As in the case of two rigid horizontal boundaries, patterns of the temperature perturbation are different in cases R_a-F_a and R_c-F_c. Maxima of the perturbation of the temperature in case R_c-F_c are located in the bulk flow, but in case R_a-F_a, on the horizontal boundaries. As was mentioned for cases R_a-R_a and R_c-R_c, thermal boundary conditions do not influence the instability mechanism, but do influence fluid velocity and the Gr_{cr}.

Convection in a Square Cavity

In the case of a laterally heated square cavity the oscillatory instability of convection is investigated for three different values of Pr: Pr = 0.015 (low-Pr fluid), Pr = 0.71 (air), and Pr = 7.0 (water). Values of Gr_{cr} and f_{cr}, obtained using from 20 to 30 basis functions in each spatial direction, are shown in Tables 3 and 4. Henkes and Hoogendoorn [16] discovered that frequency of oscillations scaled by the Brunt-Vaisala frequency $L(g\beta\Delta\theta L)^{-1/2}$ does not depend on Gr for a rather wide interval of supercritical values of Gr. The scale of the frequency used here is ν/L^2, and one can find that $f^*L(g\beta\Delta\theta L)^{-1/2} = f_{cr}/\mathrm{Gr}^{1/2}$, where f^* and f_{cr} are dimensional and nondimensional values of the critical frequency. The ratio $f_{cr}/\mathrm{Gr}^{1/2}$ is also reported in Tables 3 and 4.

Case of Low-Pr Fluid. Analysis of results obtained in the case of Pr = 0.015 (see Tables 3 and 4) confirms that accurate calculation of the critical parameters requires better spatial resolution than calculation of a stationary flow. As can be seen from Tables 3 and 4, to obtain two correct digits in values of Gr_{cr} for Pr = 0.015, more than 26 × 26 functions are necessary for conducting horizontal boundaries and 24 × 24 for adiabatic. On the other hand, values of the scaled critical frequencies $f_{cr}/\mathrm{Gr}^{1/2}$ are close for all reported truncations. Moreover, no change in the patterns of the most unstable perturbations was observed when

Table 3. Comparison of Critical Grashof Numbers and Frequencies of Oscillations with Results of Previous Work: Square Cavity with Perfectly Conducting Horizontal Walls and Heating from the Side

	Present work						Previous work		
	20 × 20	22 × 22	24 × 24	26 × 26	28 × 28	30 × 30	28 × 28 Finite element and bifurcation analysis [5]	41 × 41 Pseudo-spectral Chebyshev modes [19]	80 × 80 Finite difference mesh [16]
Pr = 0.015									
$Gr_{cr} \times 10^{-6}$	2.96	2.91	2.68	2.65	2.697	2.713	—	—	—
f_{cr}	1584.3	1581.9	1528.6	1513.6	1521.2	1525.1	—	—	—
$f_{cr}/Gr^{1/2}$	0.9209	0.9273	0.9337	0.9298	0.9263	0.9259			
Pr = 0.71									
$Gr_{cr} \times 10^{-6}$	2.972	2.973	2.9697	2.9691	2.96909	2.96907	2.9707	3.099	2.96
f_{cr}	437.12	437.21	436.93	436.91	436.91	436.91	436.98	396.1	426.7
$f_{cr}/Gr^{1/2}$	0.2536	0.253567	0.253545	0.253559	0.253561	0.253561	0.253532	0.2250	0.248
Pr = 7.0									
$Gr_{cr} \times 10^{-5}$	7.0	7.6	8.30	8.12	8.137	8.132	—	—	7.33
f_{cr}	160.8	140.9	147.0	145.3	145.55	145.46	—	—	135.3
$f_{cr}/Gr^{1/2}$	0.192	0.1616	0.1614	0.1612	0.16135	0.16130			0.158

Table 4. Comparison of Critical Grashof Numbers and Frequencies of Oscillations with Results of Previous Work: Square Cavity with Adiabatic Horizontal Walls and Heating from the Side

	Present work						Previous work	
	20 × 20	22 × 22	24 × 24	26 × 26	28 × 28	30 × 30	121 × 121 Finite difference mesh [14]	40 × 40 to 160 × 160 Finite difference mesh [16]
Pr = 0.015								
$Gr_{cr} \times 10^{-6}$	2.83	2.97	2.89	2.93	2.899	2.907	—	—
f_{cr}	1,363	1,374	1,367	1,371	1,367.1	1,368.3	—	—
$f_{cr}/Gr^{1/2}$	0.810	0.797	0.804	0.801	0.8029	0.8026		
Pr = 0.71								
$Gr_{cr} \times 10^{-8}$	0.54	0.68	0.87	1.08	1.35	1.279	2.68–2.82	2.82
f_{cr}	6,358	3,537	4,668	7,153	9,175	13,570	630	819.5 9,907
$f_{cr}/Gr^{1/2}$	0.87	0.43	0.50	0.688	0.790	1.20	0.0446	0.0488 0.590
Pr = 7.0								
$Gr_{cr} \times 10^{-8}$	—	0.34	0.41	0.31	0.402	0.392	—	5.7
f_{cr}	—	3,279	3,860	3,623	4,474	4,745	—	2,103 24,851
$f_{cr}/Gr^{1/2}$		0.56	0.60	0.65	0.706	0.758		0.088 1.04

the number of modes was increased from 18 × 18 to 30 × 30. Thus, the qualitative description of the instability is already correct for the 18 × 18 truncation, but calculation of the quantitative characteristics needs better accuracy.

Streamlines, isotherms, and isolines of the most unstable perturbation for Pr = 0.015 are shown in Figures 3b and 3c. Figure 3a illustrates the oscillatory instability for Pr = 0. Unlike the case of a long horizontal cavity, patterns of the stream function perturbation differ for different boundary conditions, as for Pr = 0 and Pr = 0.015.

In the case of Pr = 0, perturbation of the stream function (see Figure 3a) is symmetric with respect to rotation in 90° (not only 180°) around the center of the cavity. It has the maxima on the diagonals and the minimum in the center of the square. Instability onset may be described in this case as pulsations of the main convective vortex with the maxima of amplitude located near diagonals of the square between the center and all four corners.

In the case of Pr = 0.015 and perfectly conducting horizontal boundaries (see Figure 3c), perturbation of the stream function is also symmetric with respect to rotation of 90°. But perturbation of the temperature has only 180° rotation symmetry. Furthermore, perturbation of the stream function in this case rapidly increases near the boundaries. Its maxima are shifted from the diagonals and the center toward the boundaries. It is obvious that differences in the pattern of the stream function perturbation in this case and the case of Pr = 0 are caused by interaction with perturbation of the temperature, which has maxima near the

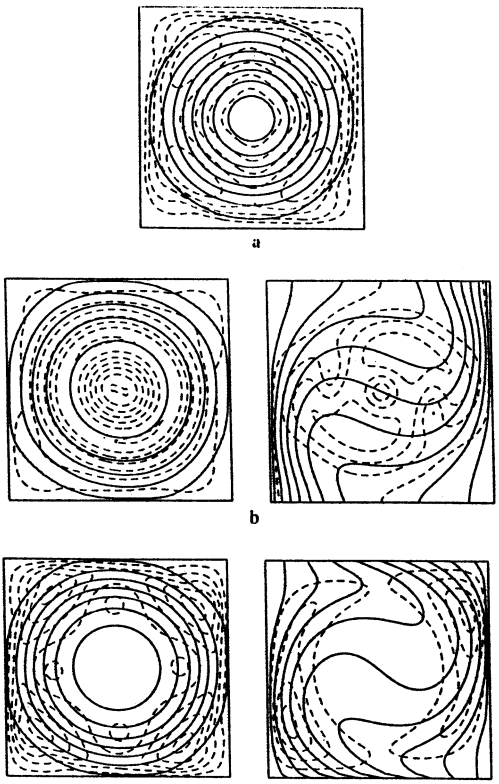

Figure 3. Streamlines and isotherms (solid lines), and the most unstable perturbations of the stream function and the temperature (dashed lines) for the case of low-Pr fluid: (a) Pr = 0, Gr = 1.09×10^6; (b) adiabatic horizontal boundaries, Pr = 0.015, Gr = 2.9×10^6; and (c) conducting horizontal boundaries, Pr = 0.015, Gr = 2.8×10^6.

vertical boundaries of the cavity. As a result, one can expect intensive oscillations of the velocity and the temperature in the boundary layer developing after onset of instability.

Completely different patterns of the most unstable perturbation characterize the onset of instability in the case of adiabatic horizontal boundaries and Pr = 0.015 (see Figure 3b). Perturbation of the temperature in this case has a maximum in the center of the cavity and is weak near the boundaries. Perturbation of the stream function has two sharp maxima in the core flow and decays rapidly toward the center as well as toward the boundaries. Convective oscillations in this case will appear in the central region of the flow, and no boundary layer effects may be expected after the onset of instability.

Comparison of the temperature perturbations in the cases of a square cavity and a cavity with $A = 4$ (see Figures 1 and 3) shows that in both cases, perturbations of the temperature have their maxima in the center of the cavity when horizontal boundaries are adiabatic, and two maxima when horizontal boundaries are perfectly conducting. As mentioned in the previous section, the instability mechanism in the case $A = 4$ is completely hydrodynamical. Similarity in the patterns of the perturbation of the temperature allows us to conclude that in the case $A = 1$, convective instability still has a hydrodynamical origin but is strongly influenced by distribution of the temperature.

Case of Perfectly Conducting Horizontal Boundaries for Pr = 0.71 and Pr = 0.7. The case of perfectly conducting horizontal boundaries and Pr = 0.71 shows the best convergence. In this case, even the 6×6 truncation used by Gelfgat [1] provided reasonable values of Gr_{cr} and f_{cr}. As follows from Table 3 for Gr_{cr}, the 20×20 basis functions provide three correct digits, and five correct digits can be obtained with 30×30 truncation. Convergence of values of the critical frequency is more rapid: five correct digits were already obtained with 26×26 truncation.

Increase of Pr from 0.71 to 7.0 for the same boundary conditions leads to much worse convergence (see Table 3). In this case, a value correct to three digits for Gr_{cr} is hardly obtained with 30×30 basis functions. But the ratio $f_{cr}/Gr^{1/2}$ already has two correct digits for 22×22 and three correct digits for 24×24 truncation, which shows that in all cases the same instability mechanism was obtained. This conclusion may be confirmed with the analysis of the most unstable perturbations, which do not show any qualitative difference when the number of basis functions is increased from 20×20 to 30×30.

Patterns of the most unstable perturbations, shown in Figure 4, may be used to explain why worse convergence is observed for higher values of Pr. Perturbation of the temperature is intensive in a thin layer near the vertical boundaries of the

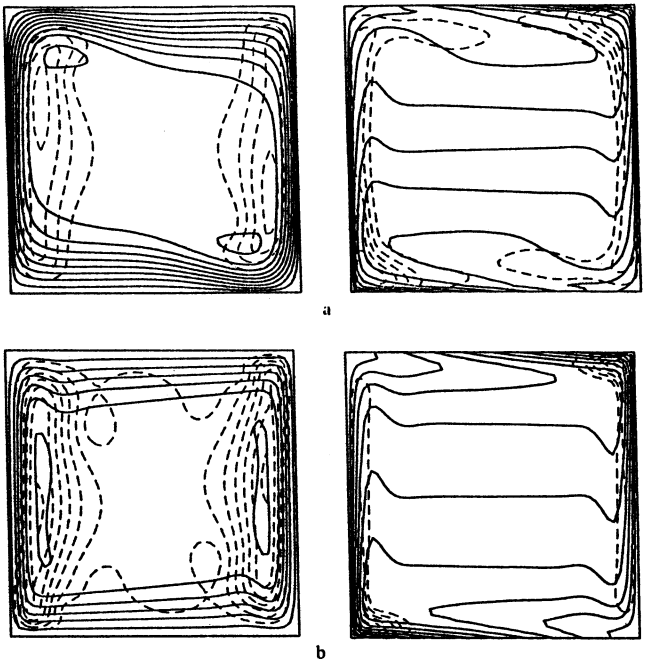

Figure 4. Streamlines and isotherms (solid lines), and the most unstable perturbations of the stream function and the temperature (dashed lines) for the case of perfectly conducting horizontal boundaries: (a) Pr = 0.71, Gr = 2.97×10^6 and (b) Pr = 7.0, Gr = 8.3×10^5.

cavity. This layer is thinner in the case of Pr = 7, and this makes polynomial approximation of the perturbation more difficult.

For Pr 0.71 and 7.0, and perfectly conducting horizontal boundaries, patterns of the most unstable perturbations are similar (see Figure 4). Both stream function and temperature perturbations are intensive near the vertical walls of the cavity and decay toward the center. Maxima of the stream function perturbation are located near maxima of the stream function, and maxima of the perturbation of the temperature occur in the lower left and upper right corners of the cavity. As already mentioned, the area near the vertical boundaries, where the perturbation is intensive, becomes thinner with increasing Pr (see Figure 4). One can conclude that larger values of Pr lead to formation of a thermal boundary layer near the vertical boundaries, where the most intensive oscillations of the temperature take place. These oscillations appear in the lower left and upper right corners, move with the convective flow along the vertical boundaries, and decay in the core region of the flow. Perturbations of the stream function in both cases are intensive in approximately the same areas near the vertical boundaries. It may be supposed that in these cases, oscillations of velocity are a sequence of the temperature oscillations appearing in the corners of the cavity.

In the case Pr = 7 the value of Gr_{cr} obtained by Henkes and Hoogendoorn [16] by straightforward simulation is smaller than the one obtained here with bifurcation analysis. It is possible that there is no contradiction between these two results. Linear stability analysis used in the present investigation gives only sufficient conditions of instability, so the real value of Gr_{cr} corresponding to finite amplitude perturbations may be less than Gr_{cr} obtained by investigation of the spectrum of the linearized equations.

Henkes and Hoogendoorn [16] related the instability mechanism illustrated in Figure 4 with the Rayleigh-Benard instability, which may be caused by an unstable local vertical temperature gradient near the left side of the lower and the right side of the upper horizontal boundaries. The present analysis shows (see Figure 4) that the maxima of the temperature perturbations are in the corners of the cavity, where the shape of the isotherms changes from almost horizontal to almost vertical. In this area both vertical and horizontal components of the temperature gradient are large, so the instability mechanism has to be connected with the interaction between unstable vertical stratification tending to move colder fluid down and hotter fluid up, and horizontal stratification tending to move all the fluid up near the hot boundary and down near the cold one.

Case of Adiabatic Horizontal Boundaries for Pr = 0.71 and Pr = 0.7. Results in the cases of Pr = 0.71 and Pr = 0.7 and adiabatic horizontal boundaries differ drastically from the previous case. No convergence was reached for either value of Pr (see Table 4). Values of Gr_{cr} obtained for 28×28 and 30×30 truncations are close, but values of f_{cr} apparently show that there is no convergence. Results of straightforward numerical simulations carried out by Henkes and Hoogendoorn [16] and Paolucci and Chenoveth [14] as well as experiments of Ivey [17] showed that, in this case, convective oscillations are observed for $Gr > 2.5 \times 10^8$ for Pr = 0.71 and $Gr > 5 \times 10^8$ for Pr = 7.

As is seen from Table 4, Gr_{cr} values are underestimated approximately by a factor of two for Pr = 0.71 and more than a factor of 10 for Pr = 7. Probable reasons for the absence of convergence may be seen from Table 5 and Figure 5.

Table 5. Results Obtained for Stationary Convection of Air in Laterally Heated Square Cavity with Adiabatic Horizontal Walls and Comparison with Results of Other Works: Pr = 0.71, Ra = Gr Pr = 10^6

	This work						Previous work		
	20 × 20	22 × 22	24 × 24	26 × 26	28 × 28	30 × 30	Benchmark solution (extrapolation using finite difference mesh from 41 × 41 to 81 × 81) [18]	65 × 65 Pseudo-spectral modes [20]	Extrapolation from 10 × 10 to 640 × 640 finite volume grid [21]
$\psi\left(\frac{1}{2},\frac{1}{2}\right)$	23.083	23.086	23.086	23.085	23.086	23.086	22.99	23.0	—
ψ_{max}	23.684	23.684	23.684	23.684	23.684	23.684	23.59	23.6	—
X_{max}, Y_{max}	0.150, 0.547	0.150, 0.547	0.150, 0.547	0.150, 0.547	0.150, 0.547	0.150, 0.547	0.151, 0.547	0.151, 0.547	
U_{max} $(x = 0.5)$	91.306	91.366	91.352	91.344	91.351	91.348	91.028	91.13	91.3193
Y_{max}	0.850	0.850	0.850	0.850	0.850	0.850	0.850	0.850	0.85036
v_{max} $(y = 0.5)$	310.73	310.82	310.82	310.82	310.83	310.83	308.96	309.8	310.508
X_{max}	0.0377	0.0377	0.0377	0.0377	0.0377	0.0377	0.0379	0.0375	0.03887
Nu_0	8.855	8.851	8.839	8.831	8.8276	8.8267	8.817	8.825	8.82513

$\psi\left(\frac{1}{2},\frac{1}{2}\right)$ is the value of the stream function at the center of the cavity, ψ_{max}, (X_{max}, Y_{max}) are the value and coordinates of the maximum stream function, U_{max} $(x = 0.5)$, Y_{max} are the value and location of the maximum horizontal velocity in cross-section $x = 0.5$, v_{max} $(y = 0.5)$, X_{max} are the value and location of the maximum vertical velocity in cross-section $y = 0.5$, and Nu_0 is the Nusselt number at the boundary $x = 0$.

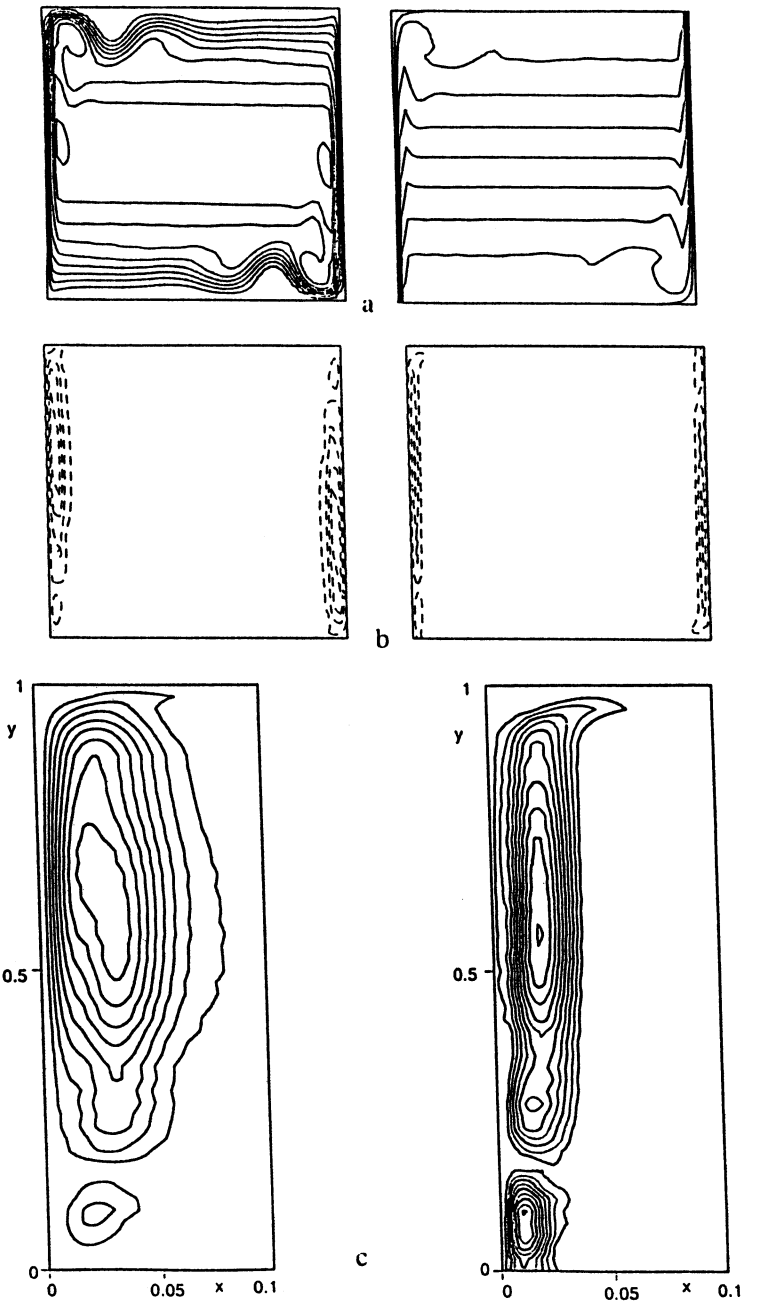

Figure 5. Results obtained for stability of convection of air (Pr = 0.71) with 30×30 truncation: (a) streamlines (left) and isotherms (right) of the convective flow, (b) isolines of the computed most unstable perturbation of the stream function (left) and the temperature (right), and (c) fragments of the most unstable perturbation for $0 < x < 0.1$.

Table 5 contains results for the test offered by de Vahl Davis [18]. Stationary convection of air (Pr = 0.71) for Ra = Gr Pr = 10^6 is considered. Analysis of the results obtained for different truncations (from 20 × 20 to 30 × 30 modes) and comparison with results of other works show very good convergence for all reported values of the stream function and velocity. However, convergence of Nu computed at the hot wall is much worse. Nu is always overestimated and decreases with the increase of number of basis functions. It is obvious that for larger values of Ra (or Gr), heat transfer through the cavity will also be overestimated, which may lead to the underestimation of the Gr_{cr}.

The reason for worse approximations of temperature than of velocity may be seen from Figure 5, where nonconverged results of stability analysis for the 30 × 30 truncation are shown. Thin temperature and velocity boundary layers (Figure 5a) are apparent. It is obvious that accurate approximation of such rapidly changing functions by smooth polynomials is very difficult. The boundary layer of the temperature is thinner than the velocity boundary layer and thus convergence of the Galerkin series of the temperature is worse. The most unstable perturbation (see Figure 5b) is also localized in the boundary layer. As one can see from fragments of the perturbation (Figure 5c) areas are very thin where perturbations are large. The characteristic width of the stream function perturbation is about 8% of the characteristic length, and the width of the temperature perturbation is approximately 2 times thinner. This obviously creates additional difficulties for the stability analysis. Boundary layers in the case of Pr = 7 are even thinner, which leads to larger errors in the values of Gr_{cr}.

DISCUSSION

In all cases when convergence was reached, the Galerkin spectral method with basis functions defined by Eqs.(7)–(10) needed fewer scalar modes than any other method used for the solution of the same problem. Even the spectral tau method with a Chebyshev basis used by Pulicani et al. [8, 9] needed more than 2 times the number of modes to obtain correct values of Gr_{cr} for the R_c-R_c case of the GAMM test.

The ability to reduce the number of modes is related to the special choice of the basis functions, which satisfy all the boundary conditions and the continuity equation. Thus, the solution is sought not in general functional space but in the subspace of divergent-free functions satisfying all the boundary conditions. Moreover, conservation properties, Eq. (15), valid for all functions belonging to this subspace are satisfied analytically. Besides decreasing the necessary number of modes, such a basis allows us to exclude pressure and avoid implicit steps connected with calculation of pressure or vorticity in the numerical procedure. It must be emphasized that the procedure used here for construction of the basis functions may be applied to any rectangular region with any linear boundary conditions if nonhomogeneity of a boundary condition is excluded by an appropriate change of variables.

It was shown that the main difficulties of application of the numerical method considered here are connected with accurate approximation of small-scale vortices and especially with thin boundary layers. It was also shown that for

investigation of instability, better spatial resolution of the flow is necessary for accurate calculation of a stationary flow. This is the same conclusion made by Winters [6, 7], who investigated GAMM test problems by the finite element method together with bifurcation analysis.

In two cases described, convergence was not reached up to a 30×30 truncation. For these cases (see Table 4), finite difference methods need more than 100 nodes in both directions. If convergence of the described Galerkin method could be reached, for example, with a 50×50 truncation, it will sufficiently decrease the amount of scalar variables.

Chebyshev polynomials were used in definition of the bases Eqs. (9) and (10) mainly because of their convenient properties, which allow us to obtain simple analytical formulas for all the necessary inner products. It is clear that smooth polynomials are not the best choice for approximation of solutions with very thin boundary layers. Better Galerkin bases may be found for such problems, but it remains completely unclear how to choose the best Galerkin basis for a given hydrodynamical problem.

APPENDIX

Formulas for coefficients α_{il}, β_{il}, f_{il}, and g_{il} are reported below.

For boundary conditions $\theta(x = 0) = \theta(x = 1) = 0$, $\alpha_{i1} = 0$, $\alpha_{i2} = -1$. For boundary conditions $\theta'(x = 0) = \theta'(x = 1) = 0$, $\alpha_{i1} = 0$, $\alpha_{i2} = -i^2/(i + 2)^2$.

For no-slip conditions $v(x = 0) = v(x = 1) = 0$,

$$f_{i1} = f_{i3} = 0$$

$$f_{02} = -\frac{8}{3} \qquad f_{i2} = -\frac{i}{(i+2)} - \frac{(i+1)(i+4)^2}{i(i+2)(i+3)} \qquad i > 0$$

$$f_{04} = \frac{4}{3} \qquad f_{i4} = \frac{(i+1)(i+4)}{i(i+3)} \qquad i > 0$$

For a stress-free upper boundary, $v(y = 0) = 0$ or $\partial v_y/\partial y(y = 1) = 0$, $v_x(y = 1) = 0$:

$$g_{01} = \frac{2}{7} \qquad g_{i1} = 2\frac{(i+1)^2}{i^3 + 5i^2 + 7i} \qquad i > 0$$

$$g_{02} = -\frac{16}{7} \qquad g_{i2} = 2\frac{i^4 + 8i^3 + 26i^2 + 40i + 24}{i^4 + 8i^3 + 22i^2 + 21i} \qquad i > 0$$

$$g_{03} = -\frac{6}{7} \qquad g_{i3} = -2\frac{i^2 + 4i + 3}{i^3 + 5i^2 + 7i} \qquad i > 0$$

$$g_{04} = \frac{4}{7} \qquad g_{i4} = \frac{i^4 + 8i^3 + 22i^2 + 27i + 12}{i^4 + 8i^3 + 22i^2 + 21i} \qquad i > 0$$

REFERENCES

1. A. Yu. Gelfgat, Numerical Realization of the Spectral Galerkin Method with Small Number of Modes for Computation of Convective Problems in Regions of Simple Geometry, *Proc. 1st ICHMT Int. Numerical Heat Transfer Conf.*, Guildford, England, pp. 167–177, 1991.
2. D. T. J. Hurle, E. Jakeman, and C. P. Jonson, Convective Temperature Oscillations in Molten Gallium, *J. Fluid Mech.*, vol. 64, part 3, pp. 565–576, 1974.
3. G. Z. Gershuni, E. M. Zhukhovitsky, and A. A. Nepomnjashchy, *Stability of Convective Flows*, Moscow, 1989.
4. F. H. Busse, Transition to Turbulence in Rayleigh-Benard Convection, in H. L. Swinney and J. P. Gollub (eds.), *Hydrodynamic Instabilities and Transition to Turbulence*, Springer-Verlag, Berlin, pp. 97–137, 1981.
5. K. H. Winters, Hopf Bifurcation in the Double-Glazing Problem with Conducting Boundaries, *J. Heat Transfer*, vol. 109, pp. 894–898, 1987.
6. K. H. Winters, Oscillatory Convection in Liquid Metals in a Horizontal Temperature Gradient, *Int. J. Numer. Methods Eng.*, vol. 25, pp. 401–414, 1988.
7. K. H. Winters, A Bifurcation Analysis of Oscillatory Convection in Liquid Metals, in B. Roux (ed.), *Numerical Simulation of Oscillatory Convection in Low-Pr Fluids: A GAMM Workshop, Notes on Numerical Fluid Mechanics*, vol. 27, pp. 319–326, 1989.
8. J. P. Pulicani and R. Peyret, Spectral Calculations of Convection in Low-Pr Fluids, in B. Roux (ed.), *Numerical Simulation of Oscillatory Convection in Low-Pr Fluids: A GAMM Workshop, Notes on Numerical Fluid Mechanics*, vol. 27, pp. 237–244, 1989.
9. J. P. Pulicani, A. Crespo del Arco, A. Randsriampianina, P. Bontoux, and R. Peyret, Spectral Simulations of Oscillatory Convection at Low Prandtl Number, *Int. J. Numer. Methods Fluids*, vol. 10, no. 5, pp. 481–517, 1989.
10. C. Canuto, M. Y. Hussaini, A. Quarteroni, and T. A. Zang, *Spectral Methods in Fluid Dynamics*, Springer-Verlag, Berlin, 1987.
11. B. Roux (ed.), *Numerical Simulation of Oscillatory Convection in Low-Pr Fluids: A GAMM Workshop, Notes on Numerical Fluid Mechanics*, vol. 27, 1989.
12. H. Ben Hadid and B. Roux, Buoyancy-Driven Oscillatory Flows in Shallow Cavities Filled with Low Prandtl Number Fluids, in B. Roux (ed.), *Numerical Simulation of Oscillatory Convection in Low-Pr Fluids: A GAMM Workshop, Notes on Numerical Fluid Mechanics*, vol. 27, pp. 25–34, 1989.
13. P. Le Quere, Contribution to the GAMM Workshop with a Pseudo-Spectral Algorithm on a Staggered Grid, in B. Roux (ed.), *Numerical Simulation of Oscillatory Convection in Low-Pr Fluids: A GAMM Workshop, Notes on Numerical Fluid Mechanics*, vol. 27, pp. 227–236, 1989.
14. S. Paolucci and D. R. Chenoveth, Transition to Chaos in a Differentially Heated Vertical Cavity, *J. Fluid Mech.*, vol. 201, pp. 379–410, 1989.
15. M. Behnia and G. de Vahl Davis, Fine Mesh Solution Using Stream Function–Vorticity Formulation, in B. Roux (ed.), *Numerical Simulation of Oscillatory Convection in Low-Pr Fluids: A GAMM Workshop, Notes on Numerical Fluid Mechanics*, vol. 27, pp. 11–18, 1989.
16. R. A. W. M. Henkes and C. J. Hoogendorn, On the Stability of the Natural Convection Flow in the Square Cavity Heated from the Side, *Appl. Sci. Res.*, vol. 47, no. 3, pp. 195–220, 1990.
17. G. N. Ivey, Experiments on Transient Natural Convection in a Cavity, *J. Fluid Mech.*, vol. 144, pp. 389–401, 1984.
18. G. de Vahl Davis, Natural Convection of Air in a Square Cavity: A Bench-Mark Solution, *Int. J. Numer. Methods Fluids*, vol. 3, pp. 249–264, 1982.

19. P. Le Quere and T. Alziary de Roquefort, On the Existence of Multiple Periodic Solutions of the Boussinesq Equations: *Mechanics of Fluids, C. R. Acad. Sci. Paris*, vol. 306, part II, pp. 681–687, 1988.
20. P. Le Quere and T. Alziary de Roquefort, Computation of Natural Convection in Two-Dimensional Cavities with Chebyshev Polynomials, *J. Comput. Phys.*, vol. 57, pp. 210–228, 1985.
21. M. Hortmann, M. Peric, and G. Scheuerer, Finite Volume Multigrid Prediction of Laminar Natural Convection: Bench-Mark Solutions, *Int. J. Numer. Methods Fluids*, vol. 11, pp. 189–207, 1990.